

Single Model Deep Learning on Imbalanced Small Datasets for Skin Lesion Classification

Peng Yao, Shuwei Shen, Mengjuan Xu, Peng Liu, Fan Zhang, Jinyu Xing, Pengfei Shao, Benjamin Kaffenberger, and Ronald X. Xu

Abstract—Deep convolutional neural network (DCNN) models have been widely explored for skin disease diagnosis and some of them have achieved the diagnostic outcomes comparable or even superior to those of dermatologists. However, broad implementation of DCNN in skin disease detection is hindered by small size and data imbalance of the publically accessible skin lesion datasets. This paper proposes a novel data augmentation strategy for single model classification of skin lesions based on a small and imbalanced dataset. First, various DCNNs are trained on this dataset to show that the models with moderate complexity outperform the larger models. Second, regularization DropOut and DropBlock are added to reduce overfitting and a Modified RandAugment augmentation strategy is proposed to address the defects of sample underrepresentation in the small dataset. Finally, a novel Multi-Weighted Focal Loss function is introduced to overcome the challenge of uneven sample size and classification difficulty. By combining Modified RandAugment and Multi-weighted Focal Loss in a single DCNN model, we have achieved the classification accuracy comparable to those of multiple ensembling models on the ISIC 2018 challenge test dataset. Our study shows that this method is able to achieve a high classification performance at a low cost of computational resources and inference time, potentially suitable to implement in mobile devices for automated screening of skin lesions and many other malignancies in low resource settings.

Index Terms—Skin lesion classification, dermoscopy, medical image analysis, deep learning.

I. INTRODUCTION

SKIN cancer is one of the most common malignancies in the world with significantly increased incidence over the past decade [1]. Skin cancer is typically diagnosed based on dermatologists' visual inspection, with support of dermoscopic imaging and confirmation of skin biopsy [2]. However, owing

Peng Yao and Shuwei Shen contributed equally to this work. Corresponding author: Ronald X. Xu.

P. Yao, M. Xu, P. Liu, F. Zhang, J. Xing, and P. Shao are with the Key Lab Precis Sci Instrument at Anhui Higher Education, University of Science and Technology of China, Hefei 230027, China (e-mail: yaopeng@ustc.edu.cn; xumj@mail.ustc.edu.cn; lpeng01@ustc.edu.cn; zxt1002@mail.ustc.edu.cn; jinyux@ustc.edu.cn; spf@ustc.edu.cn).

S. Shen is with the First Affiliated Hospital, University of Science and Technology of China, Hefei 230031, China (e-mail: swshen@ustc.edu.cn).

B. Kaffenberger is with Division of Dermatology at The Ohio State University Medical Center, Columbus 43210, USA (e-mail: benjamin.kaffenberger@osumc.edu).

R. Xu is with Department of Biomedical Engineering at The Ohio State University, Columbus, OH 43210, USA (e-mail: xu.202@osu.edu).

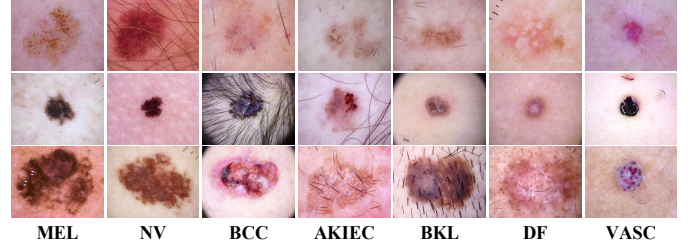


Fig. 1. Representative images of seven lesion classes in the HAM10000 dataset [3] that show variations between low inter-class and high intra-class lesions, artifacts, relatively low contrast and fuzzy borders between lesions and normal skin areas.

to the shortage of dermatologic work force and the lack of pathology lab facility in rural clinics, patients in rural communities do not have access to prompt detection of skin cancer, leading to the increased morbidities and melanoma mortalities [4]. Deep Learning (DL) based Artificial Intelligence represents a major breakthrough for computer-aided diagnosis of cancers [5]. Applying DL techniques in skin lesion classification may potentially automate the screening and early detection of skin cancer despite the shortage of dermatologists and lab facilities in rural communities [6].

Earlier approaches for computer-aided dermoscopic image analysis rely on extraction of handcrafted features to be fed into conventional classifiers [7, 8]. Recently, automatic skin cancer classification has significantly improved the performance by using end-to-end training of deep convolutional neural networks (DCNN) [9-13]. Despite these promising research progresses, practical implementation of DCNN-based dermoscopic images have achieved remarkable results, while further improvement of the diagnostic accuracy is still hindered by several limitations. *First, most of publically accessible datasets for skin lesions do not have a sufficient sample size.* Especially, in the scenario where the skin lesions have low contrast, fuzzy borders and interferences such as hair, veins or ruler marks as shown in Fig. 1, a sufficient sample size is the key for appropriate training of a DCNN model to fit the unknown data features, as exemplified by tens of millions of data for algorithm performance verification in the most commonly used ImageNet [14]. Benefited from the large training datasets, previous DCNN models have achieved significant diagnostic outcomes comparable to those of professional dermatologists [12, 13]. However, most of the training datasets for these models are derived from private datasets that are not publically accessible. In contrast, many publically available dermoscopic image datasets generally have only a few thousand samples. HAM10000 (HAM) dataset, one

TABLE I

CLASS DISTRIBUTION OF HAM. THE LESION TYPES ARE MELANOMA (MEL), MELANOCYTIC NEVUS (NV), BASAL CELL CARCINOMA (BCC), ACTINIC KERATOSIS (AKIEC), BENIGN KERATOSIS (BKL), DERMATOFIBROMA (DF), AND VASCULAR LESIONS (VASC).

	MEL	NV	BCC	AKIEC	BKL	DF	VASC
HAM	1113	6705	514	327	1099	115	142

of the largest dermoscopic image datasets, contains only 10015 images [3]. *Second, almost all the publically accessible skin disease image datasets suffering the severe data imbalance.* Since different types of skin lesions have different incident rates and imaging accessibilities, samples among different disease categories typically have uneven distributions, as shown in Table I [3]. Furthermore, many skin lesion images have low inter-class and high intra-class variations, as shown in Fig. 1 [15, 16]. These factors contribute to an imbalanced dataset and poor DCNN performance, especially for rare and similar lesion types. Therefore, it is necessary to optimize the performance of DCNNs for accurate classification of skin lesions regardless the dataset limitations.

For classification tasks on large-scale image datasets, improving the model structure from initial AlexNet [17] to RegNet [18] or increasing the parameter capacity of the similar model structures [18-20] can always achieve the better performance. However, this is not always true on small-scale image datasets since the increased parameter capacity in this case may induce transition of the models from an under-fitting area to an over-fitting area [21]. Therefore, our first set of scientific questions is: *which model structure yields the best performance and what capacity of networks in similar structures is most suitable for a small-scale dermoscopic image dataset?* Most of the previous researchers select DCNNs without detailing the scientific rationales [12, 13, 22-25]. Yu et al [15] found that a 50-layer ResNet [20] has a satisfactory performance superior to 101-layer and 38-layer ones on a dermoscopic image dataset, but they did not compare the performance variations between different DCNNs. In contrast, Santos et al [26], reported the performance differences in classification tasks for MobileNet [27], VGG-19 [28], and ResNet50 [20], but did not compare the networks of the same series. Our previous research has revealed that EfficientNet-B2 [19] has the best classification performance superior to other series of more capacity and that the increased network complexity may not be suitable for a small dermoscopic dataset [29]. In this paper, we endeavor to identify the most suitable model by comparing the classification performances of DCNNs with different structures and capacities on the HAM dataset.

In parallel with the search for the most suitable DCNN model, we also need to overcome the intrinsic limitations of the training dataset, such as the small sample size and the image artifacts that make the model prone to overfitting [30]. The second question we address in this paper is: *how to reduce overfitting of the DCNN model on a small-scale dataset with imaging artifacts?* Generally speaking, the commonly used regularization methods such as Dropout [31] can effectively alleviate overfitting [32, 33]. Ghiasi et al. have demonstrated that Dropout only works in the fully connected layer and that

DropBlock works in the convolutional layer with the contribution similar to Dropout [34]. In addition to the above methods, various data augmentation strategies, such as AutoAugment and RandAugment, have been intensively studied in the recent years as an alternative approach to reduce overfitting [35-37]. In comparison with AutoAugment, RandAugment achieves better flexibility and better performance at the lower cost of training time and computational resources. In this paper, we build a new training model by integrating Dropout and DropBlock. We also propose a modified RandAugment strategy for improved performance on dermoscopic image datasets.

In addition to model structure and data augmentation, this paper also addresses the third question associated with classification tasks on small-scale image datasets: *how to process the severely imbalanced class in a dataset?* Most commonly, the term of “imbalanced class” refers to the imbalanced distribution of sample numbers among different classes, as evidenced in the HAM dataset (Table I). This type of datasets can be processed by sample-based [38, 39] and cost-sensitive-based [40, 41] strategies. The sample-based strategy adds redundant noise data or removes informative training samples, and usually performs less effective than that of the cost-sensitive-based strategy on dermoscopic image datasets [9, 42]. In addition to imbalanced distribution of sample numbers, the term of “imbalanced class” also refers to the imbalanced classification difficulty between different classes. Lin et al. introduced a Focal Loss method to enhance the train outcome on samples with imbalanced classification difficulties [43]. Cui et al. further proposed a Class-Balanced Focal Loss function that combines the Focal Loss with the Class-Balanced Loss [44]. Considering that accurate detection of melanoma has the highest clinical impact in comparison with other skin lesion classification tasks, we propose a Multi-weighted Focal Loss method that not only overcomes the class imbalance issue in sample number and classification difficulty, but also improve the accuracy of melanoma classification by adjusting the weight of the corresponding Focal Loss.

Moreover, many previous publications show that the ensemble DCNNs usually achieve the better performance than a single-model DCNN [42, 45-49]. However, implementing ensemble DNNs in a mobile device is not practical due to storage and computational resource limitations. Therefore, we focus on using single-model DCNNs for classification tasks without involving ensemble methods.

The main contributions of this paper are thus summarized as follows:

- 1) We test the classification performance of DCNNs with different structures and capacities on the HAM dataset, and find that RegNetY-3.2GF rather than other more complicated networks achieves the best performance. This indicates that the best network for different medical image datasets needs to be re-searched in different experiments. To the best of our knowledge, this is also the first time using RegNets for dermoscopic image classification.
- 2) We redesign the DCNN model by adding regularization Dropout and DropBlock. We also propose a novel

Modified RandAugment method for improved data augmentation on the HAM dataset.

- 3) We propose a novel Multi-weighted Focal Loss method to address the class imbalance issue and to improve the accuracy for detection of key classes such as melanoma.

We have implemented the above methods to the ISIC 2018 skin lesion classification challenge test set [50] and have achieved a balanced multi-class accuracy of 0.864, ranking the fifth among all the models on the live leaderboard and the first among those with neither ensemble model nor external dataset (leaderboard data as of 1/30/2021). Our next step plan is to implement the proposed strategies to a mobile dermoscopic device for low-cost automated screening of skin diseases in low-resource settings. In addition to skin diseases, the proposed strategies can be used for low-cost and high-performance classification of many other tissue conditions. All the source codes involved in this paper are accessible upon request.

II. RELATED WORK

A. DCNN Models

Recent research and development efforts on advanced DCNN models have facilitated automated feature extraction and classification with high performance [17-20, 28, 51, 52]. He et al. introduced shortcut connections in ResNet [20] to address the degradation problem [53], making it possible to train up to hundreds or even thousands of layers. ResNet won the 2015 ImageNet image classification competition [14]. The SENet model enhanced its sensitivity to channel characteristics by introducing Squeeze-and-Excitation (SE) [51]. SENet won the 2017 ImageNet image classification competition. In 2019, Tan et al. proposed a series of lightweight DCNN models named EfficientNets [19]. Owing to their outstanding performance in many classification tasks, they have been adopted as a backbone in the latest skin lesion classification tasks [49, 54, 55]. Recently, Radosavovic et al. proposed RegNets that perform better and up to 5x faster on GPUs compared with EfficientNets of similar FLOPs and parameters [18]. RegNets consist of two sequences of RegNetXs and RegNetYs. RegNetXs were designed mainly on standard residual bottleneck block with grouped convolution, while RegNetYs were based RegNetX with the addition of SE modules [51]. In each of these series, the author trained DCNNs of FLOPs from 200M to 32G on ImageNet, and the performances of RegNetYs were better than those of RegNetXs, proving the effectiveness of the SE structure module for natural image classification.

B. Data Augmentation

Data augmentation is one of the essential keys to overcome the challenge of limited training data by randomly "augment" data diversity and number. Since the design of augmentation policies requires expertise to capture prior knowledge in each domain, it is difficult to extend existing data augmentation methods to other applications and domains. The recently emerging automatic design augmentation methods based on Learning policies is able to address the shortcomings of

traditional data augmentation methods [35-37]. Among them, the RandAugment method proposed by Cubuk et al. is the most advanced data augmentation technology so far [37]. Compared with AutoAugment [35] and Fast AutoAugment [36], the RandAugment greatly reduces the search space and thereby shorten the training time and the computational cost as well.

The search space of RandAugment consists of 14 available transformations. For transformation of each image, a parameter-free procedure is applied in order to reduce the parameter space while maintain the image diversity. RandAugment comprises 2 integer hyperparameters N and M , where N is the number of transformations applied to a training image, and M is the magnitude of each augmentation distortion. A randomly selected transformation is applied to each image according to the preset magnitude, followed by repetition of this process for $N-1$ times. All the transformations use the same global parameter M so that the resultant search space size is significantly reduced from 10^{32} as shown in AutoAugment [35] and Fast AutoAugment [36] to 10^2 .

C. Class-Balanced Loss and Focal Loss

To address the class imbalance issue in a given dataset, the cost-sensitive-based methods are commonly used. The cost-sensitive-based methods usually introduce a loss weighting factor inversely proportional to the number of samples [42]:

$$w_i = 1/N_i. \quad (1)$$

where w_i is the loss weighting factor for class i , and N_i is the number of samples for class i .

Cui et al. design a new re-weighting scheme that uses the effective number of samples for each class to re-balance the loss in Class-Balanced Loss [44]. The effective number of samples is defined as $(1 - \beta^n)/(1 - \beta)$, where n is the number of samples and $\beta \in [0:1)$ is a hyperparameter. The loss weighting factor w_i for class i is thus defined as the class-balanced loss in expression (2):

$$w_i = (1 - \beta)/(1 - \beta^{N_i}). \quad (2)$$

Notably, w_i varies in $[1, 1/N_i]$ following the change of β . As $\beta \rightarrow 1$, $w_i \rightarrow 1/N_i$. Therefore, we can finally find an optimal β value to minimize the performance loss caused by unbalanced samples among classes for any dataset.

Alternatively, Lin et al. applies a modulating term to cross-entropy loss in order to enhance the train outcome on samples with imbalanced classification difficulties [43]. First, a parameter z_i^t is defined as:

$$z_i^t = \begin{cases} z_i, & \text{if } i = y. \\ -z_i, & \text{otherwise.} \end{cases} \quad (3)$$

where z_i is the predicted value of the sample for class i , y is the ground truth. Denote $p_i^t = \text{sigmoid}(z_i^t) = 1/(1 + \exp(-z_i^t))$, the Focal Loss is then updated as:

$$\text{FL}(z, y) = -\sum_{i=1}^C (1 - p_i^t)^r \log(p_i^t). \quad (4)$$

where the parameter r smoothly adjusts the rate at which easy examples are down-weighted. As $r = 0$, the Focal Loss value

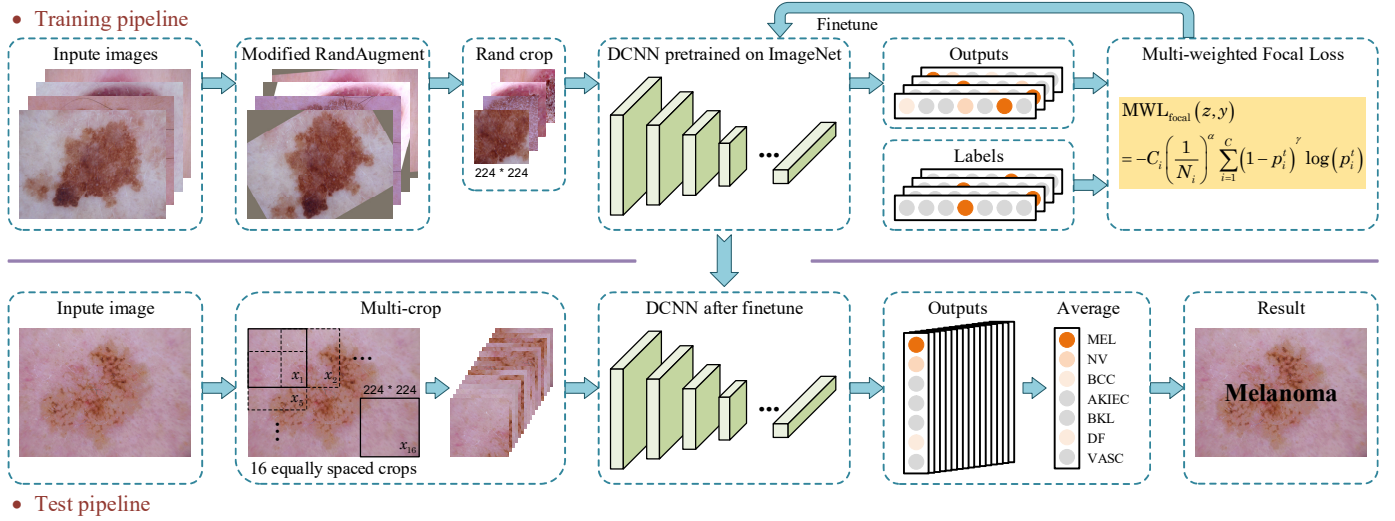


Fig. 2. The flowchart of the proposed framework. The upper part is the training pipeline, and the lower part is the test pipeline.

is equivalent to cross entropy (CE) loss. As r increases, the effect of the modulating factor increases accordingly. Based on the Class-Balanced Loss and the Focal Loss, Cui et al. further propose the Class-Balanced Focal Loss that is able to deal with the imbalances in both the sample numbers and the classification difficulties [44]. The Class-Balanced Focal Loss is expressed as following:

$$CB_{focal}(z, y) = -\frac{1-\beta}{1-\beta^{N_i}} \sum_{i=1}^C (1 - p_i')^r \log(p_i'). \quad (5)$$

III. METHODOLOGY

The proposed classification framework is illustrated by the flowchart in Fig. 2. This section first introduces the datasets and the evaluation metrics used in our study, followed by the in-depth explanation of the proposed approaches, including DCNN models, Modified RandAugment, and Multi-weighted Focal Loss method. Finally, the training and the evaluation strategies are introduced.

A. Datasets

This study uses the HAM dataset [3] for training and the ISIC 2018 challenge test dataset [50] for evaluation. The HAM dataset is the largest skin image dataset publicly available in ISIC archive.¹ It consists of 10,015 skin lesion images in seven skin lesion types, namely malignant melanoma (MEL), melanocytic nevus (NV), basal cell carcinoma (BCC), actinic keratosis (AKIEC), benign keratosis (BKL), dermatofibroma (DF) and vascular lesion (VASC), and is adopted as training dataset for ISIC 2018 skin lesion classification challenge [50]. As shown in Fig. 1 and Table I, this dataset presents with severe image interference and heavily imbalanced category distribution, significantly increasing the challenge for accurate classification between lesions. Furthermore, the test set comprises 1512 skin lesion images with the same image size as those of HAM dataset but without published labels. Therefore, the only method for performance evaluation is to upload the

predicted results to the ISIC live evaluation platform.²

B. Evaluation Metrics

In this study, the balanced accuracy (BACC) is used as the main evaluation measure, as suggested by the ISIC 2018 skin lesion classification challenge [50]. BACC is equivalent to the average sensitivity or recall and expressed as below:

$$BACC = \frac{1}{C} \sum_{i=1}^C \frac{TP_i}{TP_i + FN_i}. \quad (6)$$

where TP denotes true positives, FN denotes false negatives and C denotes the number of classes.

The conventional definition of the BACC metric treats all the classes equally, regardless the severe imbalance in difference classes. Furthermore, this metric does not reflect the clinical priority for accurate classification of life-threatening melanoma. Therefore, we also report the sensitivity of MEL, the averaged specificity and the average area under the receiver operating characteristic curve (AUC) and compare them with those of other state-of-the-art algorithms.

C. DCNN Models

In this study, we investigate DCNNs with different architectures and parameters for the best performance on HAM, a small-scale dermatoscopic image dataset. As shown in Table II, various DCNNs from the classic VGG series [28] to the latest RegNet series [18] are tested sequentially. The output dimension of the last fully connected layer (FC) of all models is modified to 7, in order to match the number of classes in the HAM dataset. According to the test results in Table IV, RegNetY-3.2GF has the best BACC value. Therefore, it is selected for all subsequent studies in this paper.

In order to further prevent overfitting, we redesign a new model, namely RegNetY-3.2GF-Drop, by inserting the DropBlock layer after Stage 3 and Stage 4, and Dropout layer before the last FC layer to the RegNetY-3.2GF model. This design is based on the rationale that DropOut only works in an FC layer and DropBlock works in a convolutional layer [34].

¹ <https://isic-archive.com/>

² <https://challenge.isic-archive.com>

TABLE II

DETAILED INFORMATION OF DCNNs WITH DIFFERENT PARAMETERS AND DIFFERENT ARCHITECTURES [18-20, 28, 51, 52].

model	params (M)	flops (B)	model	params (M)	flops (B)	model	params (M)	flops (B)
VGG-11	132.9	7.6	DenseNet-169	14.2	3.4	RegNetX-3.2GF	15.3	3.2
VGG-13	133.0	11.3	DenseNet-201	20.0	4.3	RegNetX-4.0GF	22.1	4.0
VGG-16	138.3	15.5	DenseNet-161	28.9	7.8	RegNetX-8.0GF	39.6	8.0
VGG-19	143.65	19.6	EfficientNet-b0	5.3	0.39	RegNetX-16GF	54.3	15.9
ResNet-18	11.7	1.8	EfficientNet-b1	7.8	0.7	RegNetX-32GF	107.8	31.7
ResNet-34	21.8	3.7	EfficientNet-b2	9.2	1.0	RegNetY-400MF	4.3	0.4
ResNet-50	25.6	4.1	EfficientNet-b3	12	1.8	RegNetY-800MF	6.3	0.8
ResNet-101	44.6	7.8	EfficientNet-b4	19	4.2	RegNetY-1.6GF	11.2	1.6
ResNet-152	60.2	11.5	EfficientNet-b5	30	9.9	RegNetY-3.2GF	19.4	3.2
SENet-50	28.1	4.3	EfficientNet-b6	43	19	RegNetY-4.0GF	20.6	4.0
SENet-101	49.3	7.6	EfficientNet-b7	66	37	RegNetY-8.0GF	39.2	8.0
SENet-152	66.8	11.3	RegNetX-400MF	5.2	0.4	RegNetY-16GF	83.6	15.9
SENet-154	114.3	22.6	RegNetX-800MF	7.3	0.8	RegNetY-32GF	145.0	32.3
DenseNet-121	8.0	2.9	RegNetX-1.6GF	9.2	1.6			

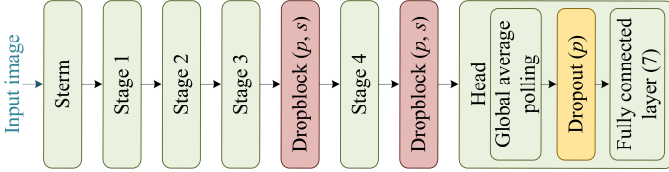


Fig. 3. The architecture of RegNetY-3.2GF-Drop

Fig. 3 shows the architecture of RegNetY-3.2GF-Drop, where the DropBlock layers share parameter s and the three regularization modules share parameter p . Here parameter p controls how many features to drop and parameter s is the size of the block to be dropped.

D. Modified RandAugment

Based on RandAugment [37], we propose a modified RandAugment strategy that is more suitable for classification tasks on dermoscopic image datasets. This strategy expands the types of transformations used in the search space of RandAugment from 14 to 21, with the intrinsic operations and the corresponding ranges of magnitude listed in Table III.

In addition to the number of transformation N and the augmentation magnitude M , the probability of executing each operation also plays an important role in training. Therefore, a probability parameter P is introduced to control whether the selected transformation should be executed or not. In order to avoid the dramatic increase of the search space scale, we share the same P value for all the operations so that each transformation has a probability of $1 - P$ to remain the original image unchanged. In addition, we found that using a random value within the allowable range performs better than using a specific amplitude M value on the HAM dataset, possibly owing to the increased diversity for transformations. Therefore, we finally use only two hyperparameters (i.e., the number of transformation N and the execution probability P) to control the data enhancement process in the Modified RandAugment strategy, leaving the amplitude of each transformation randomly selected within the allowable range.

The transformations listed in Table III is classified into 2 categories where color transformation changes the color-related properties and shape transformation changes the shape-related properties. In RandAugment, each operation is randomly selected from all the transformations without differentiating

TABLE III

LIST OF ALL TRANSFORMATIONS CAN BE CHOSEN DURING THE SEARCH.

Operation Name	Description	Range of magnitudes
Sample_Pairing [56]	Linearly add the image with another image (selected at random from the same dataset) with weight <i>magnitude</i> .	[0, 0.2]
Gauss_noise	Add random Gaussian noise to the image with weight <i>magnitude</i> .	[0, 0.2]
Saturation	Adjust the saturation. A <i>magnitude</i> =0 gives a gray image, whereas <i>magnitude</i> =1 gives the original image.	[0.6, 1.4]
Contrast	Control the contrast. A <i>magnitude</i> =0 gives a uniform gray image, whereas <i>magnitude</i> =1 gives the original image.	[0.6, 1.4]
Brightness	Adjust the brightness. A <i>magnitude</i> =0 gives a black image, whereas <i>magnitude</i> =1 gives the original image.	[0.6, 1.4]
Sharpness	Adjust the sharpness. A <i>magnitude</i> =0 gives a blurred image, whereas <i>magnitude</i> =1 gives the original image.	[0.6, 1.4]
Color_casting [57]	Randomly select a channel in RGB color spaces and add an offset value of <i>magnitude</i> .	[-30, 30]
Equalize	Equalize the histogram of each RGB channels of image respectively	
Equalize_yuv	Equalize the histogram of Y channels after transferring image into YUV color spaces	
Posterize	Reduce the number of bits for each pixel to <i>magnitude</i> bits.	[0, 3]
AutoContrast	Maximize the image contrast, by making the darkest pixel black and lightest pixel white.	
Solarize	Invert all pixels above a threshold value of <i>magnitude</i> .	[128, 255]
Vignetting [57]	Make the periphery of the image dark compared to the image center with rate <i>magnitude</i> .	[0.0, 0.6]
Rotate	Rotate the image <i>magnitude</i> degrees.	[-40, 40]
Flip	Flip image randomly in Horizontal and Vertical.	
ShearX(Y)	Shear the image along the horizontal (vertical) axis with <i>magnitude</i> degrees.	[-15, 15]
Distortion [57]	Distort the image with <i>magnitude</i> degrees.	[0.0, 0.6]
Scale	Scale the image horizontally and vertically with equal <i>magnitude</i> degrees	[0.8, 1.2]
Scale_diff	Scale the image horizontally and vertically with different <i>magnitude</i> degrees.	[0.8, 1.2]
Cutout [58]	Set a random square patch of side-length <i>magnitude</i> pixels to gray.	[0, 50]

categories [37]. Therefore, it is likely that all the operations are selected from the same category without touching the other category in the case of $N > 1$. In Modified RandAugment, we hypothesize that equivalent application of operations from both the color and the shape categories to each image will improve the training outcome. Therefore, we divide the transformations in search space into two subsets of $\{color\}$ and $\{shape\}$, comprising 13 and 8 transformations respectively. As $N > 1$, the transformations are randomly selected from $\{color\}$ and $\{shape\}$ subsets consequently. The working protocol of Modified RandAugment is illustrated below using $N = 2$ as an example:

Step 1. For each image in the training set, randomly select a transformation from $\{color\}$, and implement the transformation at the preset probability of P . If the transformation is to be performed, its amplitude is randomly selected within an allowable range. Otherwise, the original image is remained.

Step 2. Randomly select a transformation from $\{shape\}$, and follow the same procedure in Step 1 to implement the transformation.

Step 3. Randomly crop an image of 224 x 224 from the augmented image obtained from Step 2 and send it to the training network.

E. Multi-weighted Focal Loss Method

In the conventional Class-Balanced Loss method [44], the loss weighting factor w_i is calculated by (2) and the weighting strength floats within $[1, 1/N_i)$ regardless the value of β . In our

TABLE IV

BACC OF DIFFERENT DCNN MODELS ON THE ISIC 2018 SKIN LESION CLASSIFICATION CHALLENGE TEST SET.

model	BACC	model	BACC	model	BACC
VGG-11	0.769	DenseNet-169	0.836	RegNetX-3.2GF	0.842
VGG-13	0.771	DenseNet-201	0.829	RegNetX-4.0GF	0.834
VGG-16	0.745	DenseNet-161	0.837	RegNetX-8.0GF	0.831
VGG-19	0.750	EfficientNet-b0	0.838	RegNetX-16GF	0.835
ResNet-18	0.812	EfficientNet-b1	0.842	RegNetX-32GF	0.832
ResNet-34	0.825	EfficientNet-b2	0.853	RegNetY-400MF	0.839
ResNet-50	0.834	EfficientNet-b3	0.845	RegNetY-800MF	0.846
ResNet-101	0.838	EfficientNet-b4	0.842	RegNetY-1.6GF	0.850
ResNet-152	0.835	EfficientNet-b5	0.843	RegNetY-3.2GF	0.858
SENet-50	0.832	EfficientNet-b6	0.848	RegNetY-4.0GF	0.848
SENet-101	0.845	EfficientNet-b7	0.847	RegNetY-8.0GF	0.846
SENet-152	0.835	RegNetX-400MF	0.823	RegNetY-16GF	0.849
SENet-154	0.838	RegNetX-800MF	0.828	RegNetY-32GF	0.851
DenseNet-121	0.832	RegNetX-1.6GF	0.833		

Multi-weighted Focal Loss method, we modify w_i by adding the hyperparameter α , as shown in (7):

$$w_i = (1/N_i)^\alpha. \quad (7)$$

Clearly, the scope of w_i is extended beyond $[1, 1/N_i]$ as $\alpha > 1$, which will further enhance the diversity of the weighting strength. In order to reduce the sample imbalance between classes and the classification difficulty imbalance, we further combine (7) with the Focal Loss function [43] and the revised loss function is expressed in (8):

$$\text{SWL}_{\text{focal}}(z, y) = -\left(\frac{1}{N_i}\right)^\alpha \sum_{i=1}^C (1 - p_i^t)^r \log(p_i^t). \quad (8)$$

Considering the clinical priority of melanoma detection over other lesion classes, we propose a Multi-weighted Focal Loss function by added a category weighting coefficient C_i on the basis of (8). The Multi-weighted Focal Loss function is finally expressed as follow:

$$\text{MWL}_{\text{focal}}(z, y) = -C_i \left(\frac{1}{N_i}\right)^\alpha \sum_{i=1}^C (1 - p_i^t)^r \log(p_i^t). \quad (9)$$

In order to strengthen the training effect for the class of melanoma, we can simply set the category weighting coefficient C_{MEL} a value greater than 1 while keep the other C_i values as 1.

F. Training and Evaluation Strategies

The models are initialized with the weights pre-trained on the ImageNet dataset, and fine-tuned on the HAM training set [14]. As shown in Fig. 2, the proposed data enhanced strategy is applied to each image in the training set and the resultant image is randomly cropped in order to match the size of 224 x 224 required by the models.

A multi-crop strategy is adopted for evaluation of the DCNN models. As the indicated by the flowchart in Fig. 2, the areas from the upper left corner to the lower right corner of the test image are cropped with equal space, and the average of their predicted values is used as the final prediction value. The number of crops is defined as 16 in our study since we notice little improvement of the model performance beyond this number.

All the training and the testing tasks are performed on 2 NVIDIA GeForce GTX 2080Ti graphics cards using PyTorch.

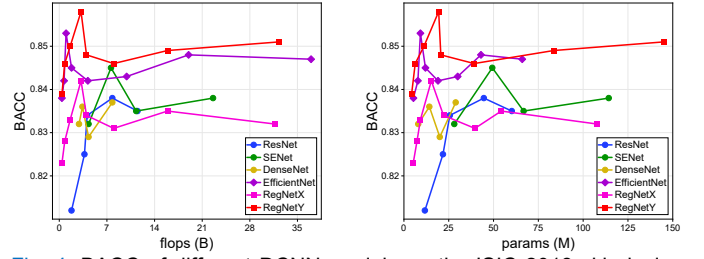


Fig. 4. BACC of different DCNN models on the ISIC 2018 skin lesion classification challenge test set (VGG models are not listed due to their poor performance).

Adam is used as an optimizer and “MultiStepLR” is used for learning rate schedule for all the models. A starting learning rate of 0.001 is chosen and is gradually reduced at a factor of $\lambda = 0.1$ per 10 epochs from the 30th epochs. In the case that the training loss cannot be reduced to a smaller value during training, a starting learning rate of 0.0001 is chosen. In order to prevent overfitting, we adopt an early stopping strategy to stop optimization after 70 epochs. Most of the models in this study use a batch size of 128. However, the batch size is reduced for some of the large models in order to match the memory capacity of the graphic cards since these models require large memory due to their feature map sizes.

IV. EXPERIMENTS AND RESULTS

A. Performance of different DCNN Models

Different DCNNs are implemented for training and testing tasks on the ISIC 2018 skin lesion classification challenge dataset. The proposed Modified RandAugment strategy and Multi-class weighted loss [42] are adopted in the training. Table IV and Fig. 4 show the performances of DCNNs in different architectures and capacities. VGG models are not listed in Fig. 4 due to their poor performance. For the models of similar architectures, such as those from Resnets to Regnets, the BACC values typically increases to a maximum value and then decreases as the capacity increases. This observation implies that, for a dataset with insufficient samples such as the HAM dataset used in this study, only the model with moderate complexity yields the best performance.

According to Table IV and Fig. 4, the most recently proposed models (e.g. EfficientNet and RegNetY) that have achieved excellent performance in general classification tasks (e.g. ImageNet) also show better performance on the ISIC2018 challenge test set. This observation implies that the DCNNs with more advanced architectures can achieve better performance than traditional ones in medical imaging tasks such as skin lesion classification. We also notice that RegNetYs generally perform better than EfficientNets. RegNetY-3.2G achieves the best 0.858 BACC, which is 0.005 higher than the best result of EfficientNet-b2. Meanwhile, RegNetYs with additional SE modules has better result than RegNetXs. The improvement in BACC validates that the addition of SE structure in DCNNs is effective for not only natural image but also dermoscopic classification tasks.

Since RegNetY-3.2G has the best BACC among all the tested models, all our subsequent experiments are carried out

TABLE V

BACC OF REGNETY-3.2GF WITH ADDING DROP-OUT AND DROP-BLOCK ON THE ISIC 2018 SKIN LESION CLASSIFICATION CHALLENGE TEST SET.

$s = 5$					
p	0.1	0.2	0.3	0.4	0.5
BACC	0.860	0.856	0.850	0.848	0.843
$p = 0.1$					
s	3	4	5	6	7
BACC	0.855	0.857	0.860	0.859	0.852

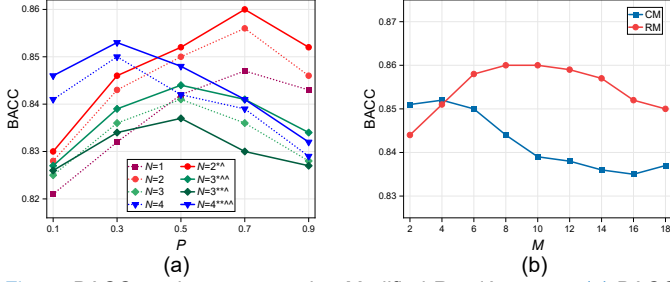


Fig. 5. BACC on the test set using Modified RandAugment. (a) BACC with different N and P . * means randomly select a transformation from the {color} subset, ^ means randomly select a transformation from the {shape} subset, and transformations are executed following the order of symbols in the training. In addition, transformation is randomly selected from the entire search space for unmarked groups. (b) BACC with the changing of M ($N=2^*$, $P=0.7$). CM is "Constant Magnitude", RM is "Random Magnitude with Increasing Upper Bound".

based on RegNetY-3.2G. As shown in Fig. 3, the DropOut and DropBlock layers are added to the RegNetY-3.2G network as the regularization methods. Table V shows the results with the unchanged training and testing setup. According to the table, BACC achieves the best value of 0.860 at $p = 0.1$ and $s = 5$, which is 0.002 higher than that of original model. In contrast, the BACC values drop below that of original RegNetY-3.2G with the further increase of p .

B. Results on Modified RandAugment

Our proposed augmentation method is validated using RegNetY-3.2G-Drop as baseline and Multi-class weighted loss as the loss function. Fig. 5 (a) shows the resultant BACCs after adopting the Modified RandAugment strategy with different N and P values. Considering the limitations in computing resources and the previous experience in RandAugment where the best N value is usually less than 4 [37], we perform the training and the testing tasks at N values ranging from 1 to 4. According Fig. 5 (a), dividing the transformations into {color} and {shape} subsets and randomly selecting transformations from the alternate subsets result in BACC values greater than randomly selecting and orderly executing transformation from the entire search space. One exception is observed for $N=3^{**}$, where the BACC value is lower than that at $N=3$.

Our experimental results show that the change of execution probability P has a significant impact on BACC. Taking $N=2^*$ as an example, BACC is only 0.832 at $P=0.1$ but reaches the best value of 0.860 at $P=0.7$. Our experimental results also show that a larger P value yields better BACC when N is small; whereas a smaller P value yields better BACC when N is large. For example, the best BACC occurs at $P=0.7$ when $N=1$ or 2, while this optimal value is achieved at $P=0.3$ when $N=4$. We

TABLE VI

BACC COMPARISON OF GENERAL AUGMENTATION MATHOD, RANDAUGMENT AND OUR MODIFIED RANDAUGMENT ON THE TEST SET.

Augment method	BACC
General Augmentation Method	0.831
RandAugment	0.850
Modified RandAugment	0.860

believe the possible reason is that keeping the ratio of transformed samples in a proper range during training helps to improve performance. If the ratio is too low, it is not conducive to increase the data diversity because more samples remain unchanged. If the ratio is too high, more samples are transformed, which is harmful to maintaining the inherent characteristics of the original samples. Therefore, when N increases, P needs to decrease accordingly in order to keep the ratio of transformed samples within an appropriate range.

In comparison with Modified RandAugment, RandAugment uses the parameter M (a single global distortion magnitude for all transformations) instead of P to optimize BACC [37]. In order to evaluate the effects of the M value on the BACC performance, we split the deformation ranges of the transformations in Table III into 10 equally spaced levels except those without an associated magnitude level. When $M = 10$, the magnitude of the transformation reaches the corresponding maximum value in Table III, and when $M > 10$, it will exceed the maximum value, indicating that the magnitude of the transformation exceeds the range of Table III. The effect of M is verified following two different schemes of "Constant Magnitude (CM)" and "Random Magnitude with Increasing Upper Bound (RM)". CM refers to a constant value for each transformation magnitude; while RM refers to a randomly selected value between 0 and M for each transformation magnitude. Fig. 5 (b) shows the BACC performance of RegNetY-3.2G-Drop after adopting the Modified RandAugment strategy and changing the M values at $N=2^*$ and $P=0.7$. According to the figure, the BACC performance of RM is superior to that of CM except at $M = 2$ or 4, indicating that a randomly distorted transformation magnitude expands the diversity of sample transformations and improves the BACC performance. In the case of RM, the BACC value does not change significantly when M is between 6 and 14, indicating that the augment effect is insensitive to the transformation magnitude within a certain range. Therefore, it is reasonable to set M as a fixed value in order to reduce the search space; and $M=10$ is used for all experiments involved in the Modified RandAugment strategy.

Table VI compares the BACC values on the test set for various DCNNs that adopt Modified RandAugment, RandAugment and general augmentation methods commonly used in DCNN trainings, such as random flipping of images, random change of brightness, contrast, saturation and hue, and random cropping. According to the table, both RandAugment and Modified RandAugment greatly improve the BACC performance, superior to the general augmentation methods. In comparison with RandAugment, Modified RandAugment further improves the BACC value by 0.01, verifying its effectiveness as a BACC improvement strategy.

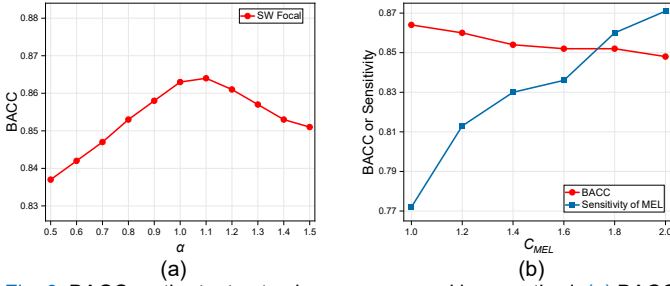


Fig. 6. BACC on the test set using our proposed loss method. (a) BACC of Single-weighted Focal Loss with different α . (b) BACC and melanoma sensitivity of Multi-weighted Focal Loss with different C_{MEL} .

TABLE VII

BACC USING DIFFERENT LOSS FUNCTIONS. BASELINE = MULTI-CLASS WEIGHTED LOSS, CB FOCAL = CLASS-BALANCED FOCAL LOSS, SW FOCAL = SINGLE-WEIGHTED FOCAL LOSS, MW FOCAL = MULTI-WEIGHTED FOCAL LOSS

Loss method	BACC	Sensitivity of melanoma
Baseline	0.860	0.760
CB Focal	0.862	0.778
SW Focal	0.864	0.772
MW Focal ($C_{MEL} = 1.2$)	0.860	0.813
MW Focal ($C_{MEL} = 1.8$)	0.852	0.860

C. Results on Multi-weighted Focal Loss

The effectiveness of our proposed Multi-weighted Focal Loss function is tested using RegNetY-3.2G-Drop as the baseline and Modified RandAugment as the augmentation method. Fig. 6 (a) shows the BACC values after adopting Single-weighted Focal Loss functions at different α levels (here another hyperparameter r is fixed as 2.0). As α increases, the value of BACC also increases until it reaches the maximum of 0.864 at $\alpha=1.1$. After that, further increase of α gradually reduces the BACC level. Noticeably, as an extension of the Class-Balanced Focal Loss [44] in weighting strength, Single-weighted Focal Loss at $\alpha=1.0$ yields a BACC value of 0.862, corresponding to the best performance achievable by Class-Balanced Focal Loss. This result verifies that Single-weighted Focal Loss is better than Class-Balanced Focal Loss in performance improvement.

Fig. 6 (b) shows the BACC and melanoma detection sensitivity performance of models adopting Multi-weighted Focal Loss of different C_{MEL} . At $C_{MEL} = 1.0$, Multi-weighted Focal Loss is equivalent to Single-weighted Focal Loss and the maximal BACC reaches 0.864, while the melanoma detection sensitivity is only 0.772. As C_{MEL} increases, the BACC decreases slightly, while the melanoma detection increases significantly. For example, as $C_{MEL} = 2.0$, BACC drops to 0.848, while melanoma sensitivity rises up to 0.871. This proves that training a DCNN with both high BACC and high sensitivity of specified class is possible by adjusting C_i .

Table VII shows the results of Multi-class weighted loss, Class-Balanced Focal Loss, Single-weighted Focal Loss, and Multi-weighted Focal Loss respectively. It is clear that the Single-weighted Focal Loss helps to achieve the best BACC, and for Multi-weighted Focal Loss, with the C_{MEL} increasing beyond 1.0, the sensitivity of melanoma is improved

significantly though the BACC value decreases slightly.

TABLE VIII

THE PERFORMANCE OF ISIC 2018 CHALLENGE WINNERS FROM THE LEGACY LEADERBOARD (ROWS 1–3), CURRENT ISIC 2018 CHALLENGE LIVE LEADERBOARD (ROWS 4–10), AND OUR PROPOSED APPROACH.

Team / authors	Use external data	Use ensemble models	BACC	Sensitivity for melanoma	Avg. AUC	Avg. specificity
Nozdryn et al. [59]	Yes	Yes	0.885	0.760	0.983	0.833
Gassert et al. [42]	Yes	Yes	0.856	0.801	0.987	0.984
Zhuang et al.	No	Yes	0.845	0.702	0.978	0.980
Minjie	Yes	Yes	0.895	0.778	0.982	0.981
Amirreza et al.	Yes	Yes	0.874	0.585	0.979	0.992
MRCN	No	-	0.872	0.860	0.953	0.979
IPM_HPC	Yes	Yes	0.866	0.830	0.976	0.976
Amirreza et al. [49]	Yes	Yes	0.862	-	0.981	-
Shen et al. [29]	No	No	0.853	0.789	0.975	0.973
Mahbod et al.	No	No	0.836	0.719	0.975	0.982
Our method ($C_{MEL}=1.0$)	No	No	0.864	0.772	0.974	0.971
Our method ($C_{MEL}=1.8$)	No	No	0.852	0.860	0.973	0.963

D. Comparison with Other Methods in the Challenge

Table VIII shows the performance of our proposed approach in comparison with those on the top of the ISIC 2018 challenge legacy leaderboard³ and the live leaderboard⁴. Besides the key metric of BACC, we also report results of sensitivity for melanoma, average specificity, and average area under the receiver operating characteristic curve (AUC) across the seven skin lesion types.

As shown in Table VIII, our proposed approach ranks fifth overall among the top 200 submissions on the live leaderboard at the time this manuscript is submitted, and surpasses the second-ranked team on the legacy leaderboard. This result ranks the first among those using a single model with additional data. In general, DCNNs with ensemble models perform better than those with a single model [42, 49, 59]. However, implementing ensemble models is less practical due to the limitation in computing resources and computing time. As an example, one of the best BACC performances on the leaderboard is achieved by integrating 90 DCNNs, which takes 13.9 seconds to classify a single test image [49]. In comparison, our method takes only 0.05 seconds in the similar computing environment, and achieves a BACC of 0.864 without using additional data, better than the ISIC leaderbaord result with additional data (BACC=0.862). Furthermore, by setting $C_{MEL} = 1.8$, we are able to reach the melanoma sensitivity of 0.860 (the highest among all ISIC submissions) at the cost of slightly decreased BACC performance.

V. CONCLUSION

This paper proposes a novel skin lesion classification strategy consisting of regularization Dropout and DropBlock, Modified RandAugment, and Multi-Weighted Focal Loss. DCNNs of different structures and capacities trained on HAM dataset show that the models with moderate complexity outperform the larger ones. The Modified RandAugment helps to achieve significant performance with less computing

³ <https://challenge.isic-archive.com/leaderboards/2018/> (TASK 3: LESION DIAGNOSIS)

⁴ <https://challenge.isic-archive.com/leaderboards/live/> (2018.3: LESION DIAGNOSIS)

resources and shorter time. The Multi-weighted Focal Loss is able to both address the class imbalance issue and improves the accuracy of key classes. By combining Modified RandAugment and Multi-weighted Focal Loss in a single DCNN model, we achieve the classification accuracy comparable to those of multiple ensembling models on the ISIC 2018 challenge test dataset. Our study shows that this method is able to achieve a high classification performance at a low cost of computational resources on a small and imbalanced dataset. It is of great potential to explore mobile devices for automated screening of skin lesions and can be also implemented in developing automatic diagnosis tools in other clinical disciplines.

REFERENCES

- [1] R. L. Siegel, K. D. Miller, and A. Jemal, "Cancer statistics, 2020," *Ca-a Cancer Journal for Clinicians*, vol. 70, no. 1, pp. 7-30, Jan, 2020.
- [2] M. E. Vestergaard, P. Macaskill, P. E. Holt, and S. W. Menzies, "Dermoscopy compared with naked eye examination for the diagnosis of primary melanoma: a meta-analysis of studies performed in a clinical setting," *British Journal of Dermatology*, vol. 159, no. 3, pp. 669-676, Sep, 2008.
- [3] P. Tschandl, C. Rosendahl, and H. Kittler, "The HAM10000 dataset, a large collection of multi-source dermoscopic images of common pigmented skin lesions," *Sci. Data*, vol. 5, pp. 1-9, Aug, 2018.
- [4] H. Feng, J. Berk-Krauss, P. W. Feng, and J. A. Stein, "Comparison of Dermatologist Density Between Urban and Rural Counties in the United States," *Jama Dermatology*, vol. 154, no. 11, pp. 1265-1271, Nov, 2018.
- [5] G. Litjens *et al.*, "A survey on deep learning in medical image analysis," *Med. Image Anal.*, vol. 42, pp. 60-88, Dec, 2017.
- [6] A. Adegun, and S. Viriri, "Deep learning techniques for skin lesion analysis and melanoma cancer detection: a survey of state-of-the-art," *Artificial Intelligence Review*, Jun 27, 2020.
- [7] J. Yang, X. Sun, J. Liang, and P. L. Rosin, "Clinical Skin Lesion Diagnosis Using Representations Inspired by Dermatologist Criteria," in *Proc. CVPR*, Jun, 2018, pp. 1258-1266.
- [8] T. Y. Satheesha, D. Satyanarayana, M. N. G. Prasad, and K. D. Dhruve, "Melanoma Is Skin Deep: A 3D Reconstruction Technique for Computerized Dermoscopic Skin Lesion Classification," *IEEE J. Transl. Eng. Health Med.*, vol. 5, pp. 1-17, 2017.
- [9] N. Gessert *et al.*, "Skin Lesion Classification Using CNNs With Patch-Based Attention and Diagnosis-Guided Loss Weighting," *IEEE Trans. Biomed. Eng.*, vol. 67, no. 2, pp. 495-503, Feb, 2020.
- [10] Y. T. Xie, J. P. Zhang, Y. Xia, and C. H. Shen, "A Mutual Bootstrapping Model for Automated Skin Lesion Segmentation and Classification," *IEEE Trans. Med. Imag.*, vol. 39, no. 7, pp. 2482-2493, Jul, 2020.
- [11] Y. D. Yuan, M. Chao, and Y. C. Lo, "Automatic Skin Lesion Segmentation Using Deep Fully Convolutional Networks With Jaccard Distance," *IEEE Trans. Med. Imag.*, vol. 36, no. 9, pp. 1876-1886, Sep, 2017.
- [12] A. Esteva *et al.*, "Dermatologist-level classification of skin cancer with deep neural networks," *Nature*, vol. 542, no. 7639, pp. 115-118, Feb, 2017.
- [13] Y. Liu *et al.*, "A deep learning system for differential diagnosis of skin diseases," *Nat. Med.*, vol. 26, no. 6, pp. 900-908, Jun, 2020.
- [14] J. Deng *et al.*, "ImageNet: A Large-Scale Hierarchical Image Database," in *Proc. CVPR*, 2009, pp. 248-255.
- [15] L. Yu, H. Chen, Q. Dou, J. Qin, and P. A. Heng, "Automated Melanoma Recognition in Dermoscopy Images via Very Deep Residual Networks," *IEEE Trans. Med. Imag.*, vol. 36, no. 4, pp. 994-1004, Apr, 2017.
- [16] J. Yang *et al.*, "Self-Paced Balance Learning for Clinical Skin Disease Recognition," *IEEE Trans. Neural Networks Learn. Syst.*, vol. 31, no. 8, pp. 2832-2846, Aug, 2019.
- [17] A. Krizhevsky, I. Sutskever, and G. E. Hinton, "ImageNet classification with deep convolutional neural networks," *Commun. ACM*, vol. 60, no. 6, pp. 84-90, Jun, 2017.
- [18] I. Radosavovic, R. Prateek Kosaraju, R. Girshick, K. He, and P. Dollár, "Designing Network Design Spaces," in *Proc. CVPR*, Jun, 2020, pp. 10425-10433.
- [19] M. Tan, and Q. V. Le, "EfficientNet: Rethinking model scaling for convolutional neural networks," in *Proc. ICML*, Jun, 2019, pp. 10691-10700.
- [20] K. He, X. Zhang, S. Ren, and J. Sun, "Deep residual learning for image recognition," in *Proc. CVPR*, Jun, 2016, pp. 770-778.
- [21] M. Belkin, D. Hsu, S. Ma, and S. Mandal. (Dec, 2018). "Reconciling modern machine learning practice and the bias-variance trade-off." [Online]. Available: <https://arxiv.org/abs/1812.11118>.
- [22] Z. Yu *et al.*, "Melanoma Recognition in Dermoscopy Images via Aggregated Deep Convolutional Features," *IEEE Trans. Biomed. Eng.*, vol. 66, no. 4, pp. 1006-1016, Apr, 2019.
- [23] S. S. Han, M. S. Kim, W. Lim, G. H. Park, I. Park, and S. E. Chang, "Classification of the Clinical Images for Benign and Malignant Cutaneous Tumors Using a Deep Learning Algorithm," *J. Invest. Dermatol.*, vol. 138, no. 7, pp. 1529-1538, Jul, 2018.
- [24] T. J. Brinker *et al.*, "Deep learning outperformed 136 of 157 dermatologists in a head-to-head dermoscopic melanoma image classification task," *Eur. J. Cancer*, vol. 113, pp. 47-54, May, 2019.
- [25] K. M. Hosny, M. A. Kassem, and M. M. Foad, "Classification of skin lesions using transfer learning and augmentation with Alex-net," *PLoS One*, vol. 14, no. 5, pp. 1-17, May, 2019.
- [26] F. P. dos Santos, and M. A. Ponti, "Robust feature spaces from pre-trained deep network layers for skin lesion classification," in *Proc. SIBGRAPI*, Dec, 2018, pp. 189-196.
- [27] A. G. Howard *et al.* (Apr, 2017). "MobileNets: Efficient Convolutional Neural Networks for Mobile Vision Applications." [Online]. Available: <https://arxiv.org/abs/1704.04861>.
- [28] K. Simonyan, and A. Zisserman, "Very deep convolutional networks for large-scale image recognition," in *Proc. ICLR*, May, 2015.
- [29] S. Shen *et al.* (Jan, 2021). "Low-cost and high-performance data augmentation for deep-learning-based skin lesion classification." [Online]. Available: <https://arxiv.org/abs/2101.02353>.
- [30] H. C. Shin *et al.*, "Deep Convolutional Neural Networks for Computer-Aided Detection: CNN Architectures, Dataset Characteristics and Transfer Learning," *IEEE Trans. Med. Imag.*, vol. 35, no. 5, pp. 1285-1298, May, 2016.
- [31] N. Srivastava, G. Hinton, A. Krizhevsky, I. Sutskever, and R. Salakhutdinov, "Dropout: A Simple Way to Prevent Neural Networks from Overfitting," *J. Mach. Learn. Res.*, vol. 15, pp. 1929-1958, Jun, 2014.
- [32] L. Wan, M. D. Zeiler, S. Zhang, Y. Lecun, and R. Fergus, "Regularization of Neural Networks using DropConnect," in *Proc. ICML*, Jul, 2013, pp. 2095-2103.
- [33] I. J. Goodfellow, D. Warde-Farley, M. Mirza, A. Courville, and Y. Bengio, "Maxout networks," in *Proc. ICML*, Jun, 2013, pp. 2356-2364.
- [34] G. Ghiasi, T.-Y. Lin, and Q. V. Le, "Dropblock: A regularization method for convolutional networks," in *Proc. NeurIPS*, Dec, 2018, pp. 10727-10737.
- [35] E. D. Cubuk, B. Zoph, D. Mané, V. Vasudevan, and Q. V. Le, "AutoAugment: Learning Augmentation Strategies From Data," in *Proc. CVPR*, Jun, 2019, pp. 113-123.
- [36] S. Lim, I. Kim, T. Kim, C. Kim, and S. Kim, "Fast AutoAugment," in *Proc. NeurIPS*, Dec, 2019.
- [37] E. D. Cubuk, B. Zoph, J. Shlens, and Q. V. Le, "RandAugment: Practical automated data augmentation with a reduced search space," in *Proc. CVPRW*, Jun, 2020, pp. 3008-3017.
- [38] N. V. Chawla, K. W. Bowyer, L. O. Hall, and W. P. Kegelmeyer, "SMOTE: Synthetic minority over-sampling technique," *J. Artif. Intell. Res.*, vol. 16, pp. 321-357, Jun, 2002.
- [39] A. Estabrooks, T. Jo, and N. Japkowicz, "A multiple resampling method for learning from imbalanced data sets," *Comput. Intell.*, vol. 20, no. 1, pp. 18-36, 2004.
- [40] C. Huang, Y. Li, C. C. Loy, and X. Tang, "Learning deep representation for imbalanced classification," in *Proc. CVPR*, Jun, 2016, pp. 5375-5384.
- [41] Z.-H. Zhou, and X.-Y. Liu, "On multi-class cost-sensitive learning," *Comput. Intell.*, vol. 26, no. 3, pp. 232-257, 2010.
- [42] N. Gessert *et al.* (Aug, 2018). "Skin Lesion Diagnosis using Ensembles, Unscaled Multi-Crop Evaluation and Loss Weighting." [Online]. Available: <https://arxiv.org/abs/1808.01694>.
- [43] T.-Y. Lin, P. Goyal, R. Girshick, K. He, and P. Dollár, "Focal Loss for Dense Object Detection," in *Proc. ICCV*, Oct, 2017, pp. 2999-3007.
- [44] Y. Cui, M. Jia, T.-Y. Lin, Y. Song, and S. Belongie, "Class-balanced loss based on effective number of samples," in *Proc. CVPR*, Jun, 2019, pp. 9260-9269.
- [45] A. Menegola, J. Tavares, M. Fornaciali, L. Tzy Li, S. Avila, and E. Valle. (Mar, 2017). "RECOD Titans at ISIC Challenge 2017." [Online]. Available: <https://arxiv.org/abs/1703.04819>.
- [46] B. Harangi, A. Baran, and A. Hajdu, "Classification Of Skin Lesions Using An Ensemble Of Deep Neural Networks," in *Proc. EMBS*, Oct, 2018, pp. 2575-2578.

- [47] B. Harangi, "Skin lesion classification with ensembles of deep convolutional neural networks," *J. Biomed. Inf.*, vol. 86, pp. 25-32, Oct, 2018.
- [48] S. S. Chaturvedi, J. V. Tembhurne, and T. Diwan, "A multi-class skin Cancer classification using deep convolutional neural networks," *Multimed. Tools Appl.*, vol. 79, pp. 28477-28498, Oct, 2020.
- [49] A. Mahbod, G. Schaefer, C. Wang, G. Dorffner, R. Ecker, and I. Ellinger, "Transfer learning using a multi-scale and multi-network ensemble for skin lesion classification," *Comput. Methods Programs Biomed.*, vol. 193, pp. 1-9, Sep, 2020.
- [50] N. Codella *et al.* (Feb, 2019). "Skin Lesion Analysis Toward Melanoma Detection 2018: A Challenge Hosted by the International Skin Imaging Collaboration." [Online]. Available: <https://arxiv.org/abs/1902.03368>.
- [51] J. Hu, L. Shen, S. Albanie, G. Sun, and E. Wu, "Squeeze-and-Excitation Networks," *IEEE Trans. Pattern Anal. Mach. Intell.*, vol. 42, no. 8, pp. 2011-2023, 2020.
- [52] G. Huang, Z. Liu, L. Van Der Maaten, and K. Q. Weinberger, "Densely connected convolutional networks," in *Proc. CVPR*, Jul, 2017, pp. 2261-2269.
- [53] R. K. Srivastava, K. Greff, and J. Schmidhuber, "Training very deep networks," in *Proc. NeurIPS*, Dec, 2015, pp. 2377-2385.
- [54] T. A. Putra, S. I. Rufaida, and J. S. Leu, "Enhanced Skin Condition Prediction Through Machine Learning Using Dynamic Training and Testing Augmentation," *IEEE Access*, vol. 8, pp. 40536-40546, 2020.
- [55] N. Gessert, M. Nielsen, M. Shaikh, R. Werner, and A. Schlaefel. (Oct, 2019). "Skin Lesion Classification Using Ensembles of Multi-Resolution EfficientNets with Meta Data." [Online]. Available: <https://arxiv.org/abs/1910.03910>.
- [56] H. Zhang, M. Cisse, Y. N. Dauphin, and D. Lopez-Paz, "MixUp: Beyond empirical risk minimization," in *Proc. ICLR*, 2018.
- [57] R. Wu, S. Yan, Y. Shan, Q. Dang, and G. Sun. (Jan, 2015). "Deep Image: Scaling up Image Recognition." [Online]. Available: <http://arxiv.org/abs/1501.02876>.
- [58] T. DeVries, and G. W. Taylor. (Aug, 2017). "Improved Regularization of Convolutional Neural Networks with Cutout." [Online]. Available: <https://arxiv.org/abs/1708.04552>.
- [59] A. Nozdryn-Plotnicki, J. Yap, and W. Yolland. (2019). "Ensembling Convolutional Neural Networks for Skin Cancer Classification." [Online]. Available: https://isic-challenge-stade.s3.amazonaws.com/dc8fd47c-1d05-489c-8b3d-f8fb18a82648/ISBI_2018.pdf?X-Amz-Algorithm=AWS4-HMAC-SHA256&X-Amz-Credential=AKIA2FPBP3IISBDRZKPE%2F20210119%2Fus-east-1%2Fs3%2Faws4_request&X-Amz-Date=20210119T082204Z&X-Amz-Expires=21600&X-Amz-SignedHeaders=host&X-Amz-Signature=007158d91af3c49f82b9d48b9fc0a6f4961c289f47017b87029f65c2d7ac768c.